Met. Mater. Int., Vol. 15, No. 5 (2009), pp. 719~725
doi: 10.1007/s12540-009-0719-3 Published 26 October 2009

Effect of Prior Microstructures on the Behavior of Cementite Particles during Subcritical Annealing of Medium Carbon Steels

Ui Gu Gang, Jong Chul Lee, and Won Jong Nam*

School of Advanced Materials Engineering, Kookmin University, Seoul 136-702, Korea

(received date: 30 April 2008 / accepted date: 31 March 2009)

The effect of prior microstructures on the behavior of cementite particles in conjunction with microstructural changes of the matrix during subcritical annealing was investigated by changing the initial microstructures into ferrite + coarse pearlite, ferrite + fine pearlite, bainite, and martensite, in medium carbon steels. While the coarsening of cementite particles in martensite proceeded rapidly with the growth of large cementite particles at boundaries with the dissolution of smaller particles within martensite laths, the coarsening rate of cementite particles in bainite was found to be much slower than that in martensite. This could be attributed to the thermal stability of cementite particles, the smaller amount of carbon in solution, and the lower driving force for solute diffusion due to the uniform size distribution of cementite particles in bainite. The controlling coarsening kinetics in medium carbon steels with ferrite-pearlite, bainite and martensite, were found as boundary diffusion, diffusion along dislocation, a combination of boundary diffusion and diffusion along dislocation, respectively.

Keywords: subcritical annealing, coarsening, kinetics, cementite, ferrite

1. INTRODUCTION

The spheroidized microstructures, with finely distributed spherical cementite particles in a ferrite matrix, have the advantage of enhancing the already excellent ductility in medium carbon steels. It is well known that the spheroidization of medium carbon steels with ferrite-pearlite structure during subcritical annealing involves the progressive disruption of lamellar cementite, the formation of spheroidal particles and the subsequent coarsening of larger particles at the expense of smaller ones. The spheroidization begins with the breakup of lamellar cementite in pearlite, and the time required for the spheroidization is significantly influenced by the breakup rate of lamellar cementite. Accordingly, most works about the spheroidization [1-8] have focused on investigations of the mechanism related to the breakup of the lamellar cementite. The introduced mechanisms, such as Rayleigh's capillarity induced perturbation theory [1-4], grain boundary thermal groove theory [5,6] and fault migration theory [4,8], are useful in describing the progressive disruption of the lamellar cementite well. However, the roles of microstructural features on spheroidizing rate are less understood. Tian, *et. al.* [9] and Shkatov, *et. al.* [10] reported that a decrease of interlamellar spacing would accelerate the spheroidization by shortening the path and raising the intensity of diffusion, whereas Chattopadhyay, *et. al.* [11] found that the rate of the spheroidization in pearlite was not significantly influenced by the variation of interlamellar spacing. According to Das, *et al.* [12], the increase of volume fraction of carbides should enhance the kinetics of cementite particle coarsening.

Meanwhile, the spheroidization of medium carbon steels with martensite or bainite structures during subcritical annealing consists of the precipitation and subsequent coarsening behavior of cementite particles. The spheroidization process of martensite is described as the following sequence: the formation of cementite particles at boundaries in the elongated form, the occurrence of uniformly distributed fine cementite particles, and the growth of large cementite particles at boundaries at the expense of the smaller intragranular particles [13,14]. For steels with carbon contents above 0.2 %C, the changes of a matrix during subcritical annealing are described as recovery with the polygonization and the annihilation of dislocations, and grain growth without recrystallization [15,16]. The behavior of the bainite structure during subcritical annealing is a little different from that of martensite. Most carbon atoms in bainite exist in the form of cementite particles [17-19]. Therefore, the coarsening rate of thermally stable cementite in bainite must be different from that in martensite. The spheroidization process of bainite has been identified as recovery, recrystallization, grain growth of

*Corresponding author: wjnam@kookmin.ac.kr

ferrite and coarsening of cementite particles [20]. According to Honeycombe and Bhadeshia [17], the bainite microstructure is much less sensitive to tempering. Therefore, it is worthwhile to compare the coarsening behavior of cementite particles during subcritical annealing for different initial microstructures of ferrite-pearlite, martensite and bainite.

Accordingly, in this work, an attempt is made to investigate the effect of prior microstructures on the behavior of cementite particles in conjunction with microstructural changes of the matrix during subcritical annealing at 973 K for medium carbon steels.

2. EXPERIMENTAL PROCEDURES

The starting materials used in this work are hot rolled wire rods of AISI 1045 with a chemical composition of 0.45 %C-0.22 %Si-0.62 %Mn-0.004 %P-0.0038 %S (in wt.%). To produce the different microtructures, rods of 10 mm in diameter were austenitized at 1173 K for 30 min followed by a quench in water (Steel D) or a salt bath set to temperatures of 653 K (Steel C), 703 K (Steel B) and 903 K (Steel A) for 1 h. For annealing treatments, the heating rate was fixed at 10 °C/min. and heating temperature was 973 K. By varying holding time at 973 K, the samples were quenched into water to investigate the spheroidizing and coarsening behavior of cementite particles.

The characteristics of the initial microstructural features, such as interlamellar spacing and the volume fraction of ferrite, were measured by linear intercept method and point counting method with a scanning electron microscope (SEM). Interlamellar spacing was an average value of the minimal interlamellar spacing measured by a linear intercept method on the colonies oriented nearly perpendicular to the plane of observation in SEM micrographs with a magnification of 8000.

For a detailed understanding of the microstructural evolution during the heat-treatment, scanning electron microscope (SEM) and transmission electron microscope (TEM) were used. Mean ferrite/pearlite interfacial area per unit volume and particle diameter of cementite particles were estimated by the lineal and aerial density analysis [21] using a rectangular grid. The grid was superimposed on the SEM micrographs with a magnification of 6000. The necessary parameters were determined: the number of intersections with surfaces per unit length of the test line, P_L, the number of interceptions of the particles per unit length of the test line, N_L, and the number of particles per unit test area, N_A. These parameters were subsequently used to measure mean interfacial area per unit volume (S_v) and particle diameter (d) using the following relationship:

$$S_v = 2P_L$$
$$d = (4/\pi)\,(N_L / N_A)$$

A quantitative analysis of the distribution of cementite particles has been performed on at least 20 SEM micrographs for each condition. The cementite particles with the aspect ratios less than 3 were considered as spheroidal particles. Specimens for TEM observation were prepared by jet polishing in a mixture solution of 5% perchloric acid and 95% acetic glacial acid.

3. RESULTS AND DISCUSSION

3.1. The distribution of cementite particles

The progressive disruption of lamellar cementite in Steel A (Fig. 1) is closely related to the breakup mechanisms [1-8]. The faster breakup of lamellar cementite and the preferential growth of cementite particles at boundaries were observed in Figs. 1(b), (c), and (d). Since the interfacial energy of particles at boundaries is lower than the surface energy of equivalent sized particles inside colonies, the solute diffusion from the matrix to boundaries caused faster growth of cementite particles at boundaries. Furthermore, since the fast growth of cementite particles at boundaries would cause the rapid consumption of the solutes, the deficiency of the solutes near boundaries resulted in the earlier breakup of lamellar cementite near boundaries (Fig. 1(c)). Additionally, the presence of denuded regions of cementite particles near boundaries (Fig. 1(d)) indicated that the larger cementite particles at boundaries would grow at the expense of the dissolution of the smaller particles near boundaries. Accordingly, it can be considered that the presence of ferrite/pearlite boundaries and pearlite colony boundaries is very effective in accelerating the breakup of lamellar cementite and the growth of cementite particles during subcritical annealing.

The comparison of microstructures of Steel A transformed at 903 K with those of Steel B transformed at 703 K will

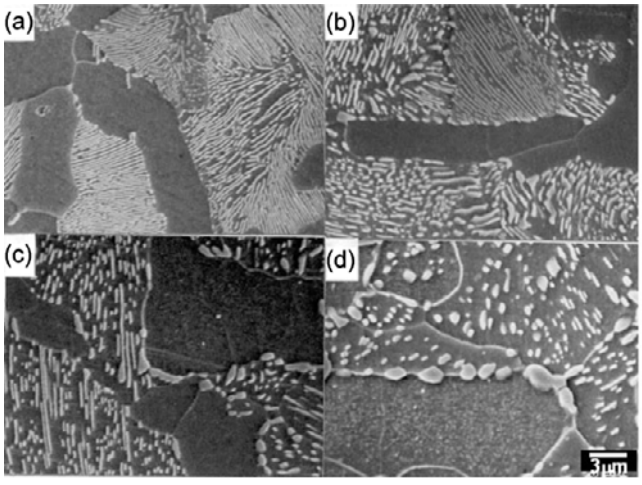

Fig. 1. SEM micrographs showing the change of the distribution of cementite particles in Steel A as a function of annealing time at 973 K: (a) as transformed, (b) 2 h, (c) 10 h, and (d) 50 h.

Table 1. Characteristic microstructural features of Steel A and Steel B

	Trans. temp.	Vol. fraction of ferrite	Mean interfacial area/Unit volume	Interlamellar spacing
Steel A	903 K	28 %	0.24 μm^{-1}	0.232 μm
Steel B	703 K	18 %	0.36 μm^{-1}	0.143 μm

give useful information about the role of the ferrite/pearlite interface as well as the interlamellar spacing during subcritical annealing (Table 1). Although ferrite volume fraction of Steel A was larger than that of Steel B, the larger width of ferrite grains in Steel A resulted in a smaller ferrite/pearlite interfacial area (0.24/μm) than that found in Steel B (0.36/μm). The mean interfacial area of ferrite/pearlite is closely related to the breakup rate of lamellar cementite and the growth of cementite particles at boundaries. Thus, more globular cementite particles at boundaries in Steel B (Fig. 2) than in Steel A (Fig. 1) indicated that the presence of boundaries will be helpful in accelerating the spheroidization of lamellar cementite. Meanwhile, the effect of interlamellar spacing could be analyzed by the investigation of the behavior of lamellar cementite inside pearlite colonies. The breakup of lamellar cementite was observed at most areas of the former pearlite region in Steel B, 0.143 μm, after only a short annealing of two hours (Fig. 2(b)), while a considerable amount of lamellar cementite still remained even after ten hours annealing in Steel A, 0.232 μm (Fig. 1(c)). Thus, it is expected that the refinement of interlamellar spacing would become an effective way of accelerating the breakup of lamellar cementite. When annealing time increased up to 50 h in Steel B, large cementite particles were bound with ferrite grain boundaries and the recrystallized and grown ferrite grains were observed (Fig. 2(d)).

The coarsening behavior of cementite particles in Steel C

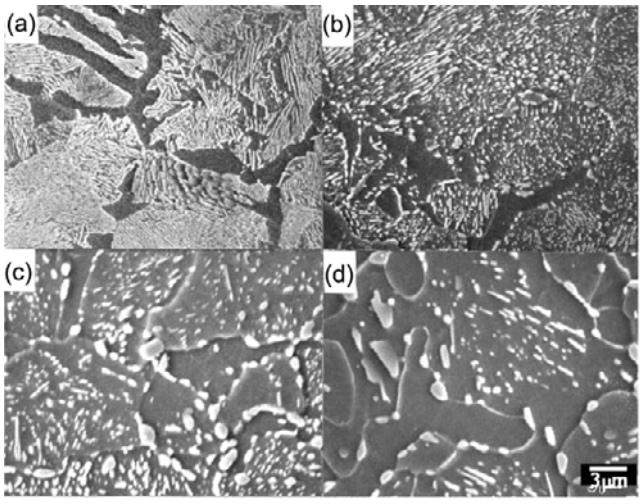

Fig. 2. SEM micrographs showing the change of the distribution of cementite particles in Steel B as a function of annealing time at 973 K: (a) as transformed, (b) 2 h, (c) 10 h, and (d) 50 h.

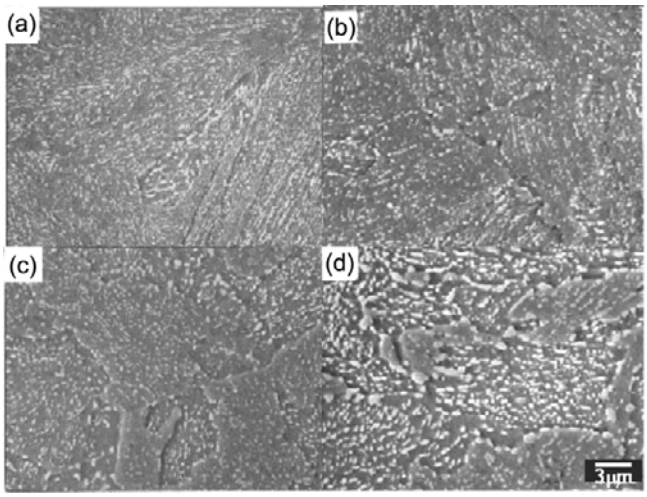

Fig. 3. SEM micrographs showing the change of the distribution of cementite particles in Steel C as a function of annealing time at 973 K: (a) as transformed, (b) 2 h, (c) 10 h, and (d) 50 h.

with bainite structure is shown in Fig. 3. Most cementite particles of similar size were located at lath boundaries, sheaf boundaries, or prior austenite boundaries (Fig. 3(a)). Thus, the reduced concentration gradients of solute atoms slowed the coarsening behavior of cementite particles during subcritical annealing. Accordingly, there was little change in the distribution and size of cementite particles up to two hours (Fig. 3(b)). Only minor changes in the morphology of the cementite particles at boundaries were observed. For ten hours annealing (Fig. 3(c)), non-uniformity of the distribution and size of cementite particles was observed. This morphology may be due to the growth of larger neighboring particles at boundaries with the dissolution of smaller boundary particles during subcritical annealing. When annealing time increased to 50 h (Fig. 3(d)), this difference became more evident. The microstructure consisted of mainly coarse cementite particles located at ferrite boundaries, and fine particles inside boundaries.

Figure 4 shows the changes of the distribution of cementite particles in Steel D during subcritical annealing at 973 K. Characteristic features of the martensite (Fig. 4(a)) are the presence of elongated regions, which are almost denuded of cementite particles. Annealing for two hours (Fig. 4(b)) reveals an increase of the size of denuded areas, although these areas retain elongated shapes, as well as maintaining the size of cementite particles at boundaries. The observed non-uniformity in the particle size may be due to an early growth of boundary particles or to the preferential growth of larger neighboring particles during subcritical annealing. Accordingly, cementite particles at boundaries are always larger than intragranular particles. After ten hours annealing (Fig. 4(c)), the presence of equiaxed ferrite grains is observed and most cementite particles are located at ferrite boundaries. A

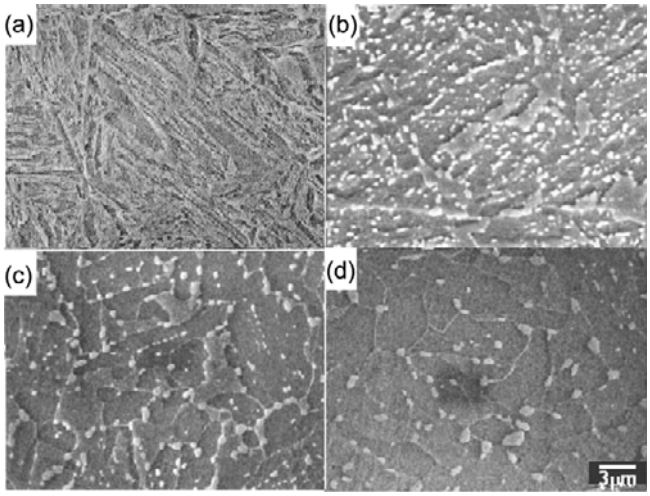

Fig. 4. SEM micrographs showing the change of the distribution of cementite particles in Steel D as a function of annealing time at 973 K: (a) as transformed, (b) 2 h, (c) 10 h, and (d) 50 h.

longer tempering time of 50 h, shown in Fig. 4(d), produces little change in the microstructure, although there is some evidences of the growth of ferrite grains and cementite particles.

3.2. Microstructural evolution of the matrix

The changes in the matrix are related to the coarsening behavior of the cementite particles. The spheroidization process of medium carbon steels with ferrite-pearlite structure during subcritical annealing is shown in Figs. 5(a), (b), (c), and (d). The progressive disruption of lamellar cementite and the occurrence of subboundaries at the region of the former lamellar cementite are observed in Steel B, which received annealing for 30 min. (Fig. 5(b)). These phenomena are quite similar to those observed in heavily drawn pearlitic steel wires [22]. In heavily drawn pearlitic steel wires, the dissolution of lamellar cementite occurs during severe deformation. However, the adjacent lamellar ferrite is bounded by interfaces without any traces of the cementite phase during annealing. These subboundaries, associated with most cementite particles, offer an effective path for the diffusion of solutes and accelerate the breakup and the formation of spheroidal cementite particles. After longer annealing of ten hours, equiaxed ferrite grains and spheroidal cementite particles as seen in Fig. 5(d) indicate that ferrite matrix is fully recystallized and the breakup of lamellar cementite is finished.

Figures 5(e), (f), (g), and (h) show the changes of bainitic microstructure during subcritical annealing. When annealed for 30 min., as shown in Fig. 5(f), the well developed substructure in the elongated form indicates the progress of recovery. All the observed cementite particles, which are either rod-shaped or spheroid, are located at subboundaries or dislocations. Most particles observed in Fig. 5(f) show lit-

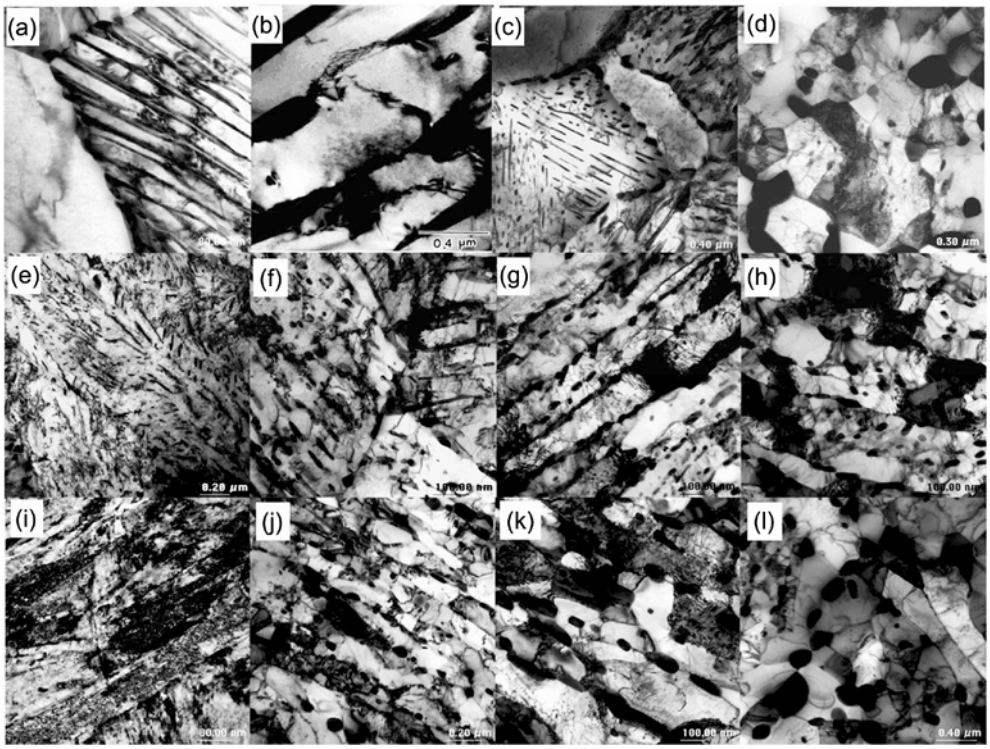

Fig. 5. TEM micrographs showing the changes of the matrix structure and the distribution of cementite particles as a function of annealing time at 973 K: (a) Steel B, as transformed; (b) Steel B, 30 min; (c) Steel B, 2 h; (d) Steel B, 10 h; (e) Steel C, as transformed; (f) Steel C, 30 min; (g) Steel C, 2 h; (h) Steel C, 10 h; (i) Steel D, as transformed; (j) Steel D, 30 min; (k) Steel D, 2 h; (l) Steel D, 10 h.

tle variation in size. When annealing time increases to two hours (Fig. 5(g)), no noticeable change in the microstructures, such as the size of cementite particles and the shape of substructures is detected. The only change that can observed in the results shown in Fig. 5(g) are the change of shape of cementite particles from the rod-type to spheroid-type, although these particles still exist as the stringers of particles, and the increased width of the substructure. After the longer annealing of ten hours, with results shown in Fig. 5(h), the presence of equiaxed subgrains is detected and the size of cementite particles connected with subboundaries is increased. Although the general features are similar to those observed in Figs. 5(d) and (l), the sizes of subgrains and cementite particles are much smaller than those in Steels B and D.

The changes of matrix structure have an influence on coarsening behavior of cementite particles during annealing of martensite. After 30 min. annealing, the substructure in the elongated form is well developed and all the cementite particles are associated with subboundaries or dislocations, as shown in Fig. 5(j). The apparent increase of the substructure width and decrease of dislocation density indicate that the polygonization and the annihilation of dislocations are operative as a recovery process. As annealing proceeds up to two hours (Fig. 5(k)), the occurrence of equiaxed subgrains is detected. It is well known that ferrite at carbon contents above 0.2 %C undergoes recovery and grain growth during tempering, without recrystallization [15,16]. Consequently, the growth of subgrains can be attributed to the annihilation of subgrain boundaries after recovery. For annealing time of ten hours, as shown in Fig. 5(l), the microstructures are similar to those observed in Fig. 5(k), except for the growth of subgrains, the smaller the dislocation density within subgrains, the more randomly distributed and large sized the cementite particles.

3.3. Coarsening kinetics of cementite particles

In investigating the coarsening kinetics of cementite particles, the simplified power law relationship between particle size and time is very useful, $d = kt^n$, where d is the average particle diameter at time t and the exponent n is a function of the controlling coarsening mechanism. The introduced coarsening kinetics are as follows: $n = 0.33$ for matrix diffusion [12,14,25-28], $n = 0.25$ for boundary diffusion [15,25,27,29], and $n = 0.20$ for diffusion along dislocations [15,29]. Meanwhile, Lindsley and Marder [15] proposed that the coarsening of cementite particles proceeds by a combination of the different coarsening mechanisms. The authors also have confirmed that the coarsening of cementite particles during tempering of martensite is controlled by a combination of the different coarsening mechanisms [30]. According to the Gibbs-Thomson equation, smaller particles have a higher concentration of the solutes than larger ones at the interface boundary. Thus, during annealing, the smaller particles go into solution and larger particles grow at the expense of the smaller ones by the diffusion of solutes down the concentration gradients in the matrix. Besides, it is generally accepted that the appropriate diffusion coefficient for the spherodization is not that of the solute, i.e., carbon in Fe-C steels, but is a coupled diffusion coefficient of carbon and iron in ferrite, although the effective diffusion coefficient can be expressed differently according to some researchers [31,32].

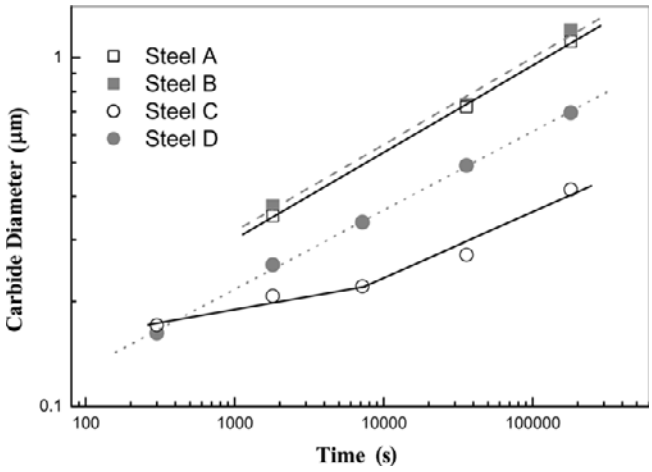

Fig. 6. A log-log plot of measured average particle diameters with annealing time.

The investigation on coarsening kinetics of cementite particles in medium carbon steels with ferrite-pearlite structure is performed only for cementite particles near boundaries by measuring the variation of the particle size with annealing time. The coarsening exponent n was determined according to the slope of the lines shown in Fig. 6. The measured n values of Steel A and Steel B are equal, at 0.249, as shown in Table 1. Since this value is close to 0.25, it can be considered that the coarsening is more significantly influenced by boundary diffusion than by matrix diffusion.

Unlike the ferrite-pearlite structure, a log-log plot of mean particle size and annealing time does not show a single linear relationship. This condition, especially the small variation in particle size at short annealing times of less than 10^4 s, cannot be explained by the application of coarsening kinetics theories. As mentioned before, the microstructural change observed in bainite after a short annealing time is only the shape-change of cementite particles without the obvious growth of the particle size. Thus, the region of short annealing time shown in Fig. 6 can be considered to be related with the spheroidization before the growth of cementite particles begins. Accordingly, the last three points in Fig. 6 were used in evaluating the coarsening kinetics of bainite, although Fig. 6 could not offer sufficient data for the analysis of the coarsening mechanism in bainite. The n value for cementite particles in Steel C, 0.200, indicates that diffusion along dislocation is the dominant mechanism for coarsening, although most

cementite particles observed in Fig. 5(g) and (h) are connected with subboundaries or dislocations.

The microstructural evolution during annealing occurs as the following sequence in martensite: at the beginning, cementite particles appear primarily at subboundaries and at prior austenite boundaries in the elongated form; other fine particles are rather uniformly distributed; these particles are replaced by large cementite particles at boundaries with time; at intermediate time both intragranular and intergranular cementite particles are observed. Ultimately the intergranular large cementite particles feed upon the smaller intragranular particles and grow. Although the average diameter of cementite particles located at the boundaries is much larger than that inside the boundaries at a short period of annealing time, this difference decreases with increasing annealing time. This is due to the dissolution of smaller intragranular particles during the growth of intergranular large cementite particles. Furthermore, all the cementite particles observed in Figs. 5(j), (k), and (l) are located at dislocations or subboundaries. Consequently, the value of 0.226 implies that both mechanisms of diffusion along dislocation and boundary diffusion would significantly contribute to the coarsening of cementite particles in Steel D.

3.4. Hardness

Figure 7 shows the variation of hardness (Hv) with annealing time for steels. During annealing and after an initial high rate of softening, steels soften continuously with an almost linear variation of hardness with log time. The hardness of Steel A is lower than that of Steel B for the whole annealing time, due to the larger volume fraction of ferrite and coarse cementite particles. It is interesting to note that Steel C with bainite structure shows the least decrease of hardness among steels, from 326 Hv to 226 Hv. Thermally stable cementite in bainite would induce a finer distribution of cementite particles and the delay of microstructural evolution due to the pinning effect of the movement of dislocations during annealing. Furthermore, there is hardly any loss of strength compared with martensite, due to the removal of the small quantity of dissolved carbon in bainite. Meanwhile, among steels Steel D shows a rapid decrease of hardness with annealing time. The initial hardness of Steel D after 5 min annealing drops 400 Hv (from 667 Hv to 267 Hv). The rapid softening of martensite during annealing can be attributed to the reduction of the higher density of dislocations as a recovery process. Additionally, the strength of martensite drops sharply as the carbon, which has a potent solid solution strengthening effect in martensite, is mostly present as coarse carbides which contribute little to strength.

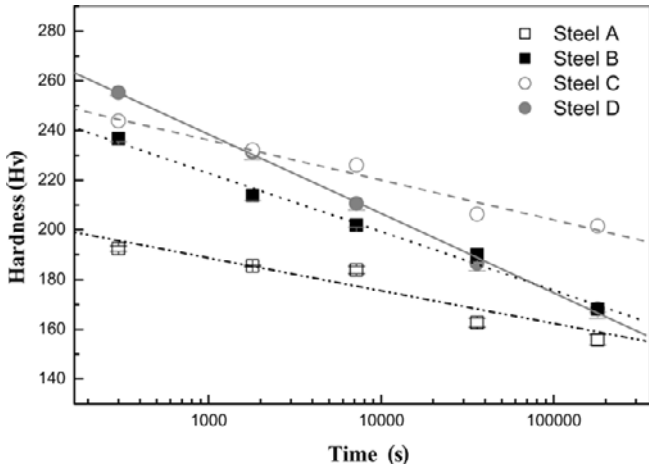

Fig. 7. The variation of hardness (Hv) with annealing time.

4. CONCLUSIONS

(1) While the coarsening of cementite particles in martensite proceeded rapidly due to the growth of large cementite particles at boundaries with the dissolution of smaller particles within martensite laths, the coarsening rate of cementite particles in bainite was found to be much slower than that in martensite. This can be attributed to the thermal stability of the cementite particles, the smaller amount of carbon in solution, and the lower driving force for solute diffusion due to the uniform size distribution of cementite particles in bainite.

(2) The controlling coarsening kinetics during subcritical annealing in medium carbon steels with ferrite-pearlite, bainite and martensite, were found to be boundary diffusion, diffusion along dislocation, a combination of boundary diffusion and diffusion along dislocation.

(3) The lower rate of softening in bainite with annealing time can be attributed to the lower density of dislocations, the lower carbon solubility in bainitic ferrite, and the thermal stability of cementite particles.

ACKNOWLEDGMENTS

This work was supported by the 2008 research fund of Kookmin University in Korea.

REFERENCES

1. Y. L. Tian and R. W. Kraft, *Met Trans. A*. **18A**, 1403 (1987).
2. E. Werner, *Acta metall*. **37**, 2047 (1989).
3. S. A. Hackney, *Scripta metall.* **25**, 799 (1991).
4. H. E. Cline, *Acta metall*. **19**, 481 (1971).
5. W. W. Mullins, *Trans. AIME*. **218**, 354 (1960).
6. Y. G. Nakagawa and G. C. Weatherly, *Met. Trans. A* **3**, 3223 (1972).
7. T. H. Courtney and J. C. M. Kampe, *Acta metall.* **37**, 1747 (1989).
8. J. C. M. Kampe, T. H. Courtney, and Y. Leng, *Acta metall*. **37**, 1735 (1989).

9. Y. L. Tian and R. W. Kraft, *Met Trans. A.* **18A**, 1359 (1987).
10. V. V. Shkatov, A. P. Chernyshev, and V. I. Lizunov, *Phys. Met. Metall.* **70**, 116 (1990).
11. S. Chattopadhyay and C.M. Sellars, *Metallography*, **10**, 89 (1977).
12. S. K. Das, A. Biswas, and R. N. Ghosh, *Acta metall. mater.* **41**, 777 (1993).
13. G. P. Airey, T. A. Hughes, and R. F. Mehl, *Trans. AIME.,* **242**, 1853 (1968).
14. T. Mukherjee, W. E. Stumpf, C. M. Sellars, and W. J. McG. Tegart, *J. Iron Steel Inst*. **207**, 621 (1969).
15. B. A. Lindsley and A. R. Marder, *Acta mater.* **46**, 341 (1998).
16. H. Kreye, *Z. Metallkde* **61**, 108 (1970).
17. R. Honeycombe and H. K. D. H. Bhadeshia, *Steels, Microstructure and Properties*, p. 131, Arnold, London (1995).
18. F. H. Samuel, *Z. Metallkde* **75**, 774 (1984).
19. Y. Ohmori, H. Ohtani, and T. Kunitake, *Metal Sci*. **8**, 357 (1974).
20. G. Deep and W. M. Williams, *Canadian Metall. Quart.* **14**, 85 (1975).
21. E. E. Underwood, *Microscope* **24**, 49 (1976).
22. J. Languillaume, G. Kapelski, and B. Baudelet, *Acta mater.* **45**, 1201 (1997).
23. I. M. Lifshitz and V. V. Slyozov, *J. Phys. Chem. Solids*. **19**, 35 (1961).
24. C. Wagner, *Z. Elektrochem*. **65**, 581 (1961).
25. R. W. Heckel and R. L. DeGregorio, *Trans. AIME*. **233**, 2001 (1965).
26. G. P. Airey, T. A. Hughes, and R. F. Mehl, *Trans. AIME*. **242**, 1853 (1968).
27. K. M. Vedula and R. W. Heckel, *Met. Trans*. *A* **1**, 9 (1970).
28. R. T. DeHoff and C. V. Iswaran, *Met. Trans. A* **13**, 1389 (1982).
29. A. J. Ardell, *Acta metall*. **20**, 601 (1972).
30. W. J. Nam and C. M. Bae, *Scripta mater.* **41**, 31 (1999).
31. R. A. Oriani, *Acta metall*. **12**, 1399 (1964).
32. C. Li, J. M. Blakely, and A. H. Feingold, *Acta metall*. **14**, 1397 (1966).